Research Article

Fatemeh Yaghoubi, Seyed Morteza Naghib, Najmeh Sadat Hosseini Motlagh, Fateme Haghiralsadat, Hossein Zarei Jaliani, Davood Tofighi, and Ali Moradi*

Multiresponsive carboxylated graphene oxide-grafted aptamer as a multifunctional nanocarrier for targeted delivery of chemotherapeutics and bioactive compounds in cancer therapy

https://doi.org/10.1515/ntrev-2021-0110
received September 8, 2021; accepted October 19, 2021

Abstract: To date, the use of nanocarriers has been developed in various fields, especially in cancer treatment. Graphene oxide (GO) is a novel drug delivery system that eagerly attracts the attention of many researchers due to its unique features. For the first time, a biocompatible AS1411 APT-GO-COOH was synthesized for the co-delivery of chemotherapeutics and herbal drugs. Here, a human gastric adenocarcinoma cell line (AGS) was targeted with aptamer-carboxylated graphene oxide (APT-CGO) containing anticancer drugs (curcumin (CUR) and doxorubicin (DOX)). The current study aimed to assess the anti-cancer effect of combination therapy, as well as target genes and proteins interfering in the development of gastric cancer. After attachment of APT to CGO, the drugs (CUR and DOX) were loaded on the carrier, establishing a co-delivery system. Then, physical characteristics, release profile, cytotoxicity assay, cellular uptake, expression rates of the genes (RB1, CDK2, AKT, and NF-KB) and proteins (RB1, CDK2), and the apoptosis rate were determined. The designed co-delivery system for the drugs (CUR and DOX) and APT showed a thermo- and pH-sensitive drug release behavior that successfully reduced the expression of CDK2, AKT, and NF-KB while it enhanced RB1 expression at the gene and protein levels. Also, APT-CGO-drugs were successfully targeted to the AGS cell line, leading to a highly inhibitory property against this cell line compared to CGO-drugs. It seems that the co-delivery of CUR and DOX along with APT as a targeting agent was more effective than CGO-drugs, suggesting a promising candidate for the treatment of gastric cancer. The results showed that this biofunctionalized nanocarrier could reduce the cytotoxicity of the drugs in normal cells and could increase efficiency.

Keywords: graphene oxide, curcumin, doxorubicin, aptamer, cell culture, drug delivery, nanoparticle

* **Corresponding author: Ali Moradi,** Department of Clinical Biochemistry, School of Medicine, Shahid Sadoughi University of Medical Sciences, Yazd, Iran, e-mail: morady2008@gmail.com, tel: +98-9126706056
Fatemeh Yaghoubi: Department of Clinical Biochemistry, School of Medicine, Shahid Sadoughi University of Medical Sciences, Yazd, Iran; Herbal Medicine Research Center, Faculty of Pharmacy, Shahid Sadoughi University of Medical Sciences, Yazd, Iran
Seyed Morteza Naghib: Nanotechnology Department, School of Advanced Technologies, Iran University of Science and Technology (IUST), P.O. Box 16846-13114, Tehran, Iran
Najmeh Sadat Hosseini Motlagh: Dapartment of Biomedical Engineering, Meybod University, Meybod, Iran
Fateme Haghiralsadat: Department of Advanced Medical Sciences and Technologies, School of Paramedicine, Shahid Sadoughi University of Medical Sciences, Yazd, Iran; Medical Nanotechnology & Tissue Engineering Research Center, Department of Advanced Medical Sciences and Technologies, Yazd Reproductive Sciences Institute, Shahid Sadoughi University of Medical Sciences, Yazd, Iran
Hossein Zarei Jaliani: Department of Medical Biotechnology, School of Medicine, Shahid Sadoughi University of Medical Sciences, Yazd, Iran
Davood Tofighi: Epidemiology, and Research Design Support (BERD), Clinical and Translational Science Center, Department of Psychology, University of New Mexico, Albuquerque, New Mexico, United States of America

1 Introduction

Despite common strategies for the treatment of cancer (surgery, chemotherapy, and radiotherapy), it remains a major cause of morbidity and mortality worldwide [1,2]. Although the efficiency of chemotherapy has been proved in recent years, the serious obstacle is its side effects on normal cells and toxicity [3]. Also, extensive heterogeneity of tumor cells and drug resistance count as other

Open Access. © 2021 Fatemeh Yaghoubi *et al.*, published by De Gruyter. This work is licensed under the Creative Commons Attribution 4.0 International License.

obstacles in cancer treatment, which cause the efflux of anticancer agents from cancer cells [4]. In fact, heterogeneity is derived from DNA instability and epigenetic differences of tumor cells, leading to diverse responses to therapy. Therefore, combination therapy can be applied as an effective strategy due to targeting several pathways of cancer cells [5]. Nanotechnology and bioactive nanomaterials established a revolution in biomedicine and biotechnology [6–10]. Nanocarriers have attracted the attention of many researchers in the last few years [11–13], owing to their great advantages such as reducing the systemic toxicity of the loaded drugs, as well as their ability to deliver several drugs, simultaneously [14–18].

Doxorubicin (DOX), a common chemotherapeutic agent [19–21], causes DNA double-helical breaks that inhibit the growth of tumor cells and induce apoptosis [22]. A single use of free DOX in the elimination of cancer cells is ineffective due to its broad side effects including cardiotoxicity, myelosuppression, elimination of the normal cells, and premature inactivation [23]. Owing to the anti-cancer properties of plant-derived compounds, they are widely used as effective agents in the treatment of various cancers. Curcumin (CUR) is a flavonoid found in herbal remedies and dietary turmeric that possesses anti-inflammatory, anti-oxidant, and anti-cancerous properties [24]. Moreover, CUR is a polyphenol extracted from *Curcuma longa* in 1815, which has acquired much consideration of researchers in the world for its bioactivities including antiviral, antimicrobial, anti-inflammatory, and antioxidant activities (for treatment of several chronic diseases such as cancers, neurodegenerative diseases, obesity, liver disease, metabolic syndrome, arthritis, and inflammation). The antitumor capability of CUR has been much discussed recently and still is still widely researched [25]. CUR acts through several cell signaling pathways, including inflammation (IL-1, IL-6, NF-kB, COX-2, and 5-LOX), proliferation (HER-2, AP-1, and EGFR), apoptosis (reduction of anti-apoptotic gene and activation of caspases) and angiogenesis (VEGF) [26]. In response to DNA damage, the RB1 gene activates cell cycle arrest by controlling the transition from G1/G0- to S-phase in the cell cycle [27].

Low absorption and solubility, fast metabolism, and rapid removal of CUR from the body are some restrictions in the administration of CUR [28,29]. Therefore, multiple nanocarriers have been developed in the last decades to overcome such limitations. The high capacity for the high loading of different molecules, such as metals and biomolecules through the planar structure of graphene, makes it a suitable nanocarrier. Graphene oxide (GO) can not only carry small drug molecules and macromolecules but also carry either hydrophilic or hydrophobic substances due to its bipolar groups. These excellent properties and high biocompatibility made GO a promising candidate for medical applications [30]. For enhancing the biocompatibility and solubility of GO, the functionalization of GO was conducted *via* the addition of some groups, such as carboxyl [31]. Safety, efficacy and higher biocompatibility of drugs loaded onto GO-COOH have been shown in previous studies [32,33].

Wu *et al.* showed more cytotoxicity of GO/DOX compared to pure DOX against human multiple myeloma cells [34]. Another study evaluated the release profile of CUR from PEGylated GO, which was dependent on pH, and the release increased in a basic environment [35]. Also, co-loading of CUR and Paclitaxel on polymer-functionalized reduced GO showed a synergistic effect and was highly potent against A549, MDA-MB-231, and lung cancer cells [36].

This study aimed to target the AGS cell line by APT AS1411 and to improve the cytotoxicity effect of CUR by co-delivery with DOX. As a result, the cytotoxicity effect, cellular uptake, expression rates of RB1, AKT, NF-KB, and CDK2 genes, expression rates of RB1 and CDK2 proteins, and flow cytometry analysis have been studied (Scheme 1).

2 Materials and methods

2.1 Reagents

PBS tablets, dialysis bag (MW¼ 12 kDa), MTT (3-(4,5-dimethylthiazol-2-yl)-2,5-diphenyl tetrazolium bromide), DMSO (dimethyl sulfoxide), and CUR (purity >65%) were obtained from Sigma-Aldrich (St Louis, MO, USA). DOX was supplied from Ebewe Pharma (Australia). DAPI (40, 6-diamidino-2-phenylindole) and DIL stain (1,10-dioctadecyl-3,3,30,30-tetramethylindocarbocyanine perchlorate) were purchased from Thermo Fisher Scientific (Waltham, MA, USA). GO was purchased from GrapheneX. The sequences of AS1411 was HEX-5′-(GGTGGTGGTGGTTGTGGTGGTGGTGG)-3′-NH_2 purchased from Pishgam (Iran). Actin, RB, and CDK2 mouse monoclonal antibody were supplied from Santa Cruz (Texas, USA). Annexin V-FITC/propidium iodide (PI) apoptosis detection kit was supplied from Abcam (Cambridge, UK).

2.2 Morphological characterization

The zeta potential of CGO and APT-CGO was evaluated by Brookhaven Corp Instruments (Holtsville, NY, USA).

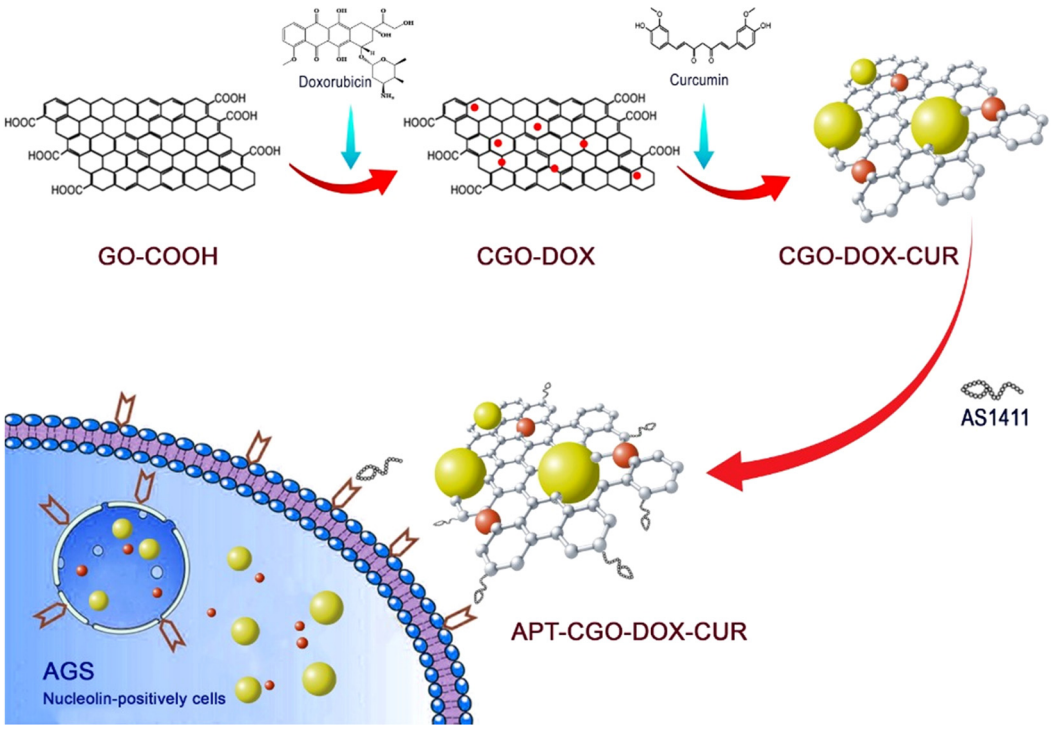

Scheme 1: Illustration of the synthesis procedure of the functionalized GO (APT-CGO) and its application in cancer therapy.

Also, a scanning electron microscope (SEM) was used to observe the CGO structure. For this purpose, a thin layer of film was required that was produced by pouring 5 µL of suspension on a glass plate. Finally, the sample was coated with a gold layer and the images were captured by SEM (model EM3200, KYKY, China).

2.3 Preparation of GO-COOH

The following steps were applied to carboxylation of GO: sonication of GO (2 mg mL^{-1}) for 1 h, addition of 72 mg of NaOH, stirring at room temperature for 4 h, addition of 0.4 mL of HCl (37% v/v), washing the suspension with deionized water, and centrifuging at 4,000 g for removing the salts [37].

2.4 Conjugation of APT to CGO

AS1411 APT was linked to CGO by the amide formation between –COOH group of GO and –NH_2 section of APT, through coupling 1-ethyl-3-(3-dimethylaminopropyl)-carbodiimide (EDC) and *N*-hydroxysuccinimide (NHS). First, 1 mg mL^{-1} of CGO mixed with 5 mM EDC and 10 mM NHS in PBS at pH 7.4 were stirred for 3 h. Then, 500 µL of APT (1 µM) was added to the solution and stirred overnight at room temperature. Finally, APT-CGO was collected with centrifugation and washed three times with deionized water [38].

2.5 Preparation of a drug delivery system

For drug loading on the CGO, CUR (0.5 mg mL^{-1} in ethanol) and DOX (0.5 mg mL^{-1} in PBS) were mixed with CGO (1 mg mL^{-1}), and stirred overnight at room temperature. For co-loading of drugs, CGO (1 mg mL^{-1}) was mixed with CUR (0.5 mg mL^{-1}) and DOX (0.5 mg mL^{-1}) at the same ratio (1:1). Unbounded drugs were removed by centrifuging at 15,000*g* for 10 min, while a UV-Vis spectrophotometer (Epoch Box 998 America) was used to calculate their concentration by assessing the absorption of CUR and DOX at 430 and 480 nm, respectively. Ultimately, entrapment efficiency (EE%) was measured using the following equation:

$$EE\% = (\text{Loaded drug on GO-COOH (mg mL}^{-1}) / \text{Total drug (mg mL}^{-1})) \times 100.$$

2.6 Drug release assay

For assessing the release behavior of CUR and DOX from CGO, a 12 kDa cut-off dialysis tube containing drug loaded onto CGO, was immersed in PBS at pH 7.4 and 5.5 at 37°C

and 42°C, while stirring for 72 h. At different time intervals, the dialysis solution (0.5 mL) was gathered for measuring its absorbance by the UV-Vis spectrophotometer, and substituted with fresh PBS (0.5 mL). According to the total loaded drug concentration, the percentage of release was evaluated at different times.

2.7 Cell culture assay

AGS cell line was supplied from Pasteur Institute (Tehran, Iran). The cells were cultured in DMEM (Gibco, Grand Island) containing penicillin–streptomycin (Gibco, Grand Island) and 10% fetal bovine serum (FBS) (Gibco Grand Island) under standard conditions (37°C and 5% CO_2).

2.8 *In vitro* evaluation of cellular uptake

Fluorescence intensity was measured for detecting the distribution of the following formulations in the cells: APT-CGO, CGO-CUR, APT-CGO-CUR, CGO-DOX, APT-CGO-DOX, and APT-CGO-CUR-DOX. For this purpose, the cells were cultured in a 6-well plate (1.5×10^5 per well). After 24 h, the cells were incubated with the listed formulations for 3 h. Then, the cells were washed and fixed with PBS (pH 7.4) and 95% ethanol solution, respectively. Ultimately, the cells were stained with DAPI (1 mg mL^{-1}), and the images were recorded using a fluorescence microscope (Olympus, Japan).

2.9 Cytotoxicity study

MTT assay was applied to measure IC_{50} doses of blank GO-COOH (62.5, 125, 250, 500, and 1,000 μM), free DOX, APT-CGO-DOX (0.31, 0.625, 1.25, 2.5, 5, and 10 μg mL^{-1}), free CUR and APT-CGO-CUR (3.9, 7.8, 15.6, 31.25, 62.5, and 125 μg mL^{-1}) after 48 h. Also, IC_{50} of the combination form of drugs on CGO was calculated at different concentrations (4.1, 8.125, 16.25, 32.5, 65, and 130 μg mL^{-1}). The content of wells was removed when incubation of each well was executed with 90 μL of themedium and 10 μL of MTT (5 mg mL^{-1}) for 3 h. Afterward, the formazan crystals were dissolved in DMSO. Finally, an EPOCH spectrophotometer (Bio-Tek, Winooski) was used for measuring the absorbance of the samples at 570 nm.

2.10 Real-time PCR

Assessment of the expression of RB1 and CDK2 genes involved in the cell cycle, AKT1 involved in the signal transduction, and NF-KB involved in the cell survival, was performed by Real time PCR. The AGS cell line was seeded in a 6-well plate, and 150,000 cells per well were incubated with free CUR, free DOX, free CUR-DOX, APT-CGO-CUR, APT-CGO-DOX, and APT-CGO-CUR-DOX. The medium was removed after 48 h and washed with PBS. RNX-Plus extraction kit was used for extraction of total RNA. Consequently, cDNA synthesis was performed using the Parstous cDNA synthesis kit. Then, quantitative real-time PCR was performed through specific primers for CDK2, AKT1, RB1, NF-KB genes and Beta-actin (a housekeeping gene), and Yekta-tajhiz master mix. The following protocol was used for the synthesis of cDNA (for 40 cycles): 95°C for 1 min, 95°C for 5 s, 60°C for 20 s, 72°C for 10 s, and 72°C for 2 min. Finally, the rate expression of CDK2, AKT1, RB1, and NF-KB genes was assessed using the $2^{-\Delta\Delta CT}$ method. The primer sequences of the related genes are shown in Table 1.

2.11 Western blot analysis

AGS cells were seeded in a 6-well plate and allowed to reach 80% confluence. Then, the cells were treated with free APT, free CUR, free DOX, free CUR-DOX, APT-CGO, CGO-CUR, APT-CGO-CUR, CGO-DOX, APT-CGO-DOX, and APT-CGO-CUR-DOX for 48 h. The cells were lysed with

Table 1: The primer sequences of real-time PCR

Gene	Forward (5′-3′)	Reverse (5′-3′)	Product length (bp)
Beta-actin	CGCGAGAAGATGACCCAGATC	GATAGCACAGCCTGGATAGCAAC	77
RB1	CAGAAGCCATTGAAATCTACCTC	GGTGTGCTGGAAAAGGGTCC	147
CDK2	GCTTTTGGAGTCCCTGTTCG	GGTCCCCAGAGTCCGAAAGA	111
AKT1	TCTATGGCGCTGAGATTGTG	CTTAATGTGCCCGTCCTTGT	113
NF-KB	TACTCTGGCGCAGAAATTAGGTC	CTGTCTCGGAGCTCGTCTATTTG	157

RIPA buffer, and their protein concentration was calculated by Bradford assay. Then, 10% SDS-PAGE was applied for 50 µg of samples. After at least 2 h, the bands were transferred into a nitrocellulose membrane that was incubated with 5% BSA for 1 h at room temperature to stop nonspecific binding. Then, 1:1,000 dilution of every β-actin, RB, and CDK2 primary antibody were incubated with the membranes overnight at 4°C. A horseradish peroxidase-conjugated secondary antibody (1:2,000) was applied for probing the bands for 2 h at room temperature. Ultimately, the ECL kit (GE Healthcare) was used for the visualization by a chemiluminescence visualization system (Syngene GBOX Gel Documentation 680X).

2.12 Flow cytometry analysis

Cell apoptosis was evaluated with an Annexin V-FITC/PI apoptosis analysis kit. For this purpose, after culturing the cells in 6-well plates and reaching 80% confluence, the cells were treated with free APT, free CUR, free DOX, free CUR-DOX, APT-CGO, CGO-CUR, APT-CGO-CUR, CGO-DOX, APT-CGO-DOX, and APT-CGO-CUR-DOX. After 48 h, total cells were collected by trypsinization, centrifuged, and washed with PBS. Then, 100 µL of binding buffer was added and stained with Annexin V-FITC and PI. After 15 min, the rate of apoptotic cells was quantified with a flow cytometer (BD Biosciences, USA).

3 Results and discussion

3.1 Characterization

The surface morphology of CGO is depicted in Figure 1a, which shows the sheet layer and broad surface of CGO [39,40]. In the physiological system, surface charge expressed as zeta potential plays a key role in cellular interactions that is determined by dynamic light scattering (DLS). Indeed, the amount of zeta potential determines repulsion or attraction between the particles [41]. A higher positive or a negative value of zeta potential indicates greater stability (particles are dispersed). In contrast, at a lower value of zeta potential, aggregation is formed [42,43]. The negative zeta potential of CGO (−75.0 mV) was attributed to the presence of −COOH group on its surface (Figure 1b). After binding of APT, the charge level of CGO was increased from −75 to −42.9, which confirmed the binding of APT. Also, energy-dispersive X-ray analysis (EDX) was performed for determining the elemental compositions of CGO and APT-CGO. Due to the presence of nitrogen and phosphate elements in APT, the amount of these elements increased 3.5 and 10 times, respectively, in APT-CGO, rather than CGO, confirming successful binding of APT (Table 2).

FTIR spectra of the prepared nanomaterials are shown in Figure 1c. The broad band of OH appeared at ~3,240 cm^{-1}, as well as a functional group of GO-COOH (C═C) appeared at ~1,631 cm^{-1} [44]. Covalent conjugation of APT was confirmed by FTIR (Figure 1c). After conjugation with APT, the amide bond was formed at 1,725 cm^{-1} (C═O) and 1,382 cm^{-1} (C–N).

Figure 1d–e displays the UV-Vis spectra of free APT, free CUR, free DOX, APT-CGO, APT-CGO-CUR, CGO-DOX, and APT-CGO-DOX. The characteristic absorption peaks of free CGO, APT, and CUR appeared at 230, 260, and 430 nm, respectively, which were in good agreement with previous studies [38,39]. After conjugation of APT, an absorption peak appeared at 255 nm, while the related peak for CGO was absent, verifying the conjugation of A1 with GO. In APT-CGO/CUR, the specific peak of CUR appeared at 430 nm. Also, in APT-CGO/DOX, the maximum absorbance of DOX was observed at 480 nm.

3.2 Loading assay

The potency of CGO as sheet-like nanoparticles for co-delivery of the hydrophobic drug (CUR) and hydrophilic drug (DOX), which have shown an anticancer effect, was assessed [45,46]. The loading of CUR and DOX, in separate or combined form, was conducted by simple mixing of APT-CGO with CUR and DOX overnight. Then, unbound drugs were removed by centrifugation while loaded ones were measured by UV-vis absorbance at 430 and 480 nm for CUR and DOX, respectively. Although the loaded CUR and DOX were visible according to their colors (yellow and red, respectively), in fact, CUR and DOX were linked to APT-CGO *via* π–π stacking interactions, as reported previously [45,47]. The pH of CGO has a key role in the maximum loading of drugs. The pH of drugs is close to the pH of CGO (5.5–6) and so the higher loading is achieved. The % EE values of CUR and DOX were 80.8 and 88.4% in the separate form, while in the combined form, was 81.6 and 92.8%, respectively.

3.3 Release assay

The release profiles of CGO-CUR and APT-CGO-CUR or CGO-DOX and APT-CGO-DOX were similar, verifying

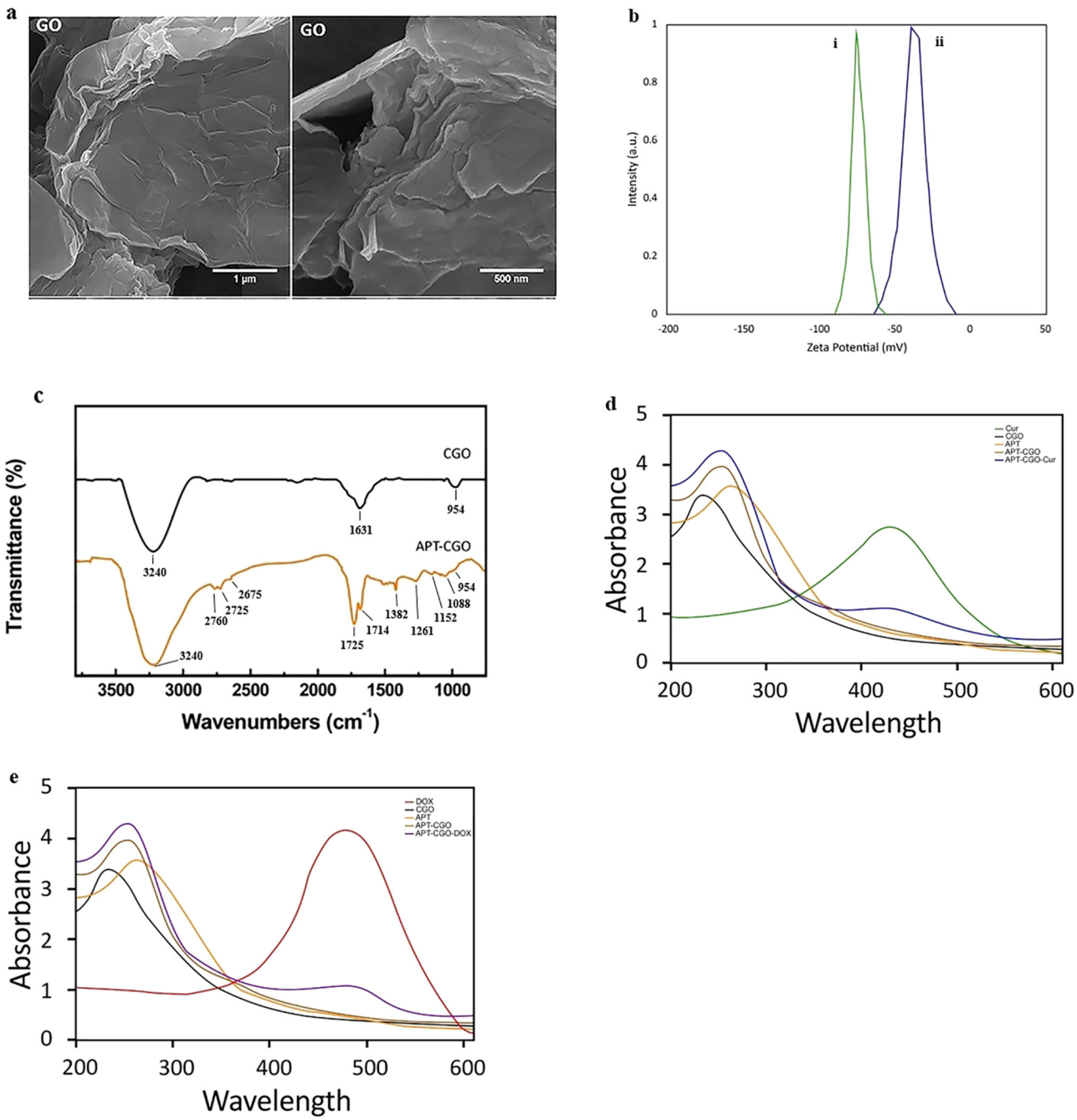

Figure 1: (a) SEM images of CGO. (b) Zeta potential of CGO and APT-CGO. (c) FTIR of CGO and APT-CGO. (d) UV-Vis spectra of CUR, CGO, APT, APT-CGO, and APT-CGO-CUR. (e) UV-Vis spectra of DOX, CGO, APT, APT-CGO, and APT-CGO-DOX.

that there was no effect of APT on the release rate of CUR and DOX. In general, cancerous cells have higher temperatures and lower pH than normal cells [48]. Indeed, the pH and temperature of the surrounded environment of nanocarriers have an impact on the rate of drug release. Therefore, pH 7.5/temperature 37°C and pH 5.5/temperature 42°C were selected for normal and cancer cells, respectively. Based on the obtained results, the designed formulation has shown thermo- and pH-sensitive properties. The highest release rates of CUR and DOX, in an acidic condition at pH 5.5 and a temperature of 42°C, were 14.97 and 81.36%, respectively (Figure 2). In fact, acidic pH enhances the solubility of CUR resulting in decreased interactions between the drug and CGO [49]. In contrast, the lowest release rate was attributed to physiological conditions. High temperatures weaken the $\pi \rightarrow \pi^*$

Table 2: Zeta potential and EDX analysis of CGO and APT-CGO

	Zeta potential (mV)	EDX analysis	
		% N	*% P*
CGO	−75.0	3.6	0.06
APT-CGO	−42.9	12.8	0.6

bonds and at acidic pH, the amine ($-NH_2$) groups of DOX would be protonated resulting in the decrease of hydrogen-bonding interaction [44]. As shown in Figure 2(c and d), the release of CUR and DOX renders in the combined form compared to the separate form. The obtained results were similar to those of Omidi *et al.*, Malekmohammadi *et al.*, and Pourjavadi *et al.* [43,50,51]. This thermo- and pH-sensitive drug release profile suggested a good advantage to enhance the drug release from nanocarriers for anticancer drug delivery applications, leading to increased therapeutic efficiency of the designed system.

3.4 Cellular uptake assay

A targeted drug-delivery system must be able to target specific tumor cells. Nucleolin overexpressing cells, such as AGS, were targeted by AS1411, which was evaluated by a cellular uptake assay *in vitro*. In the current study, free DOX and CUR as well as loaded ones on APT-CGO were co-cultured with the AGS cell line. DIL, DiIC18, and DAPI (4′,6-diamidino-2-phenylindole) dyes were used for staining CGO and the nuclei of cancer cells, respectively. The successful delivery of APT-CGO, CGO-CUR, APT-CGO-CUR, CGO-DOX, APT-CGO-DOX, and APT-CGO-CUR-DOX are depicted in Figure 3. CUR, DOX, and APT were monitored as green, red, and orange fluorescence, respectively. The free form of the drugs showed fluorescence intensity similar to that of the loaded form. The free forms pass into the cells by two pathways: diffusion mechanism through the cell membrane, and endocytosis that is counted as a key route for the loaded drugs [52]. When the drugs are

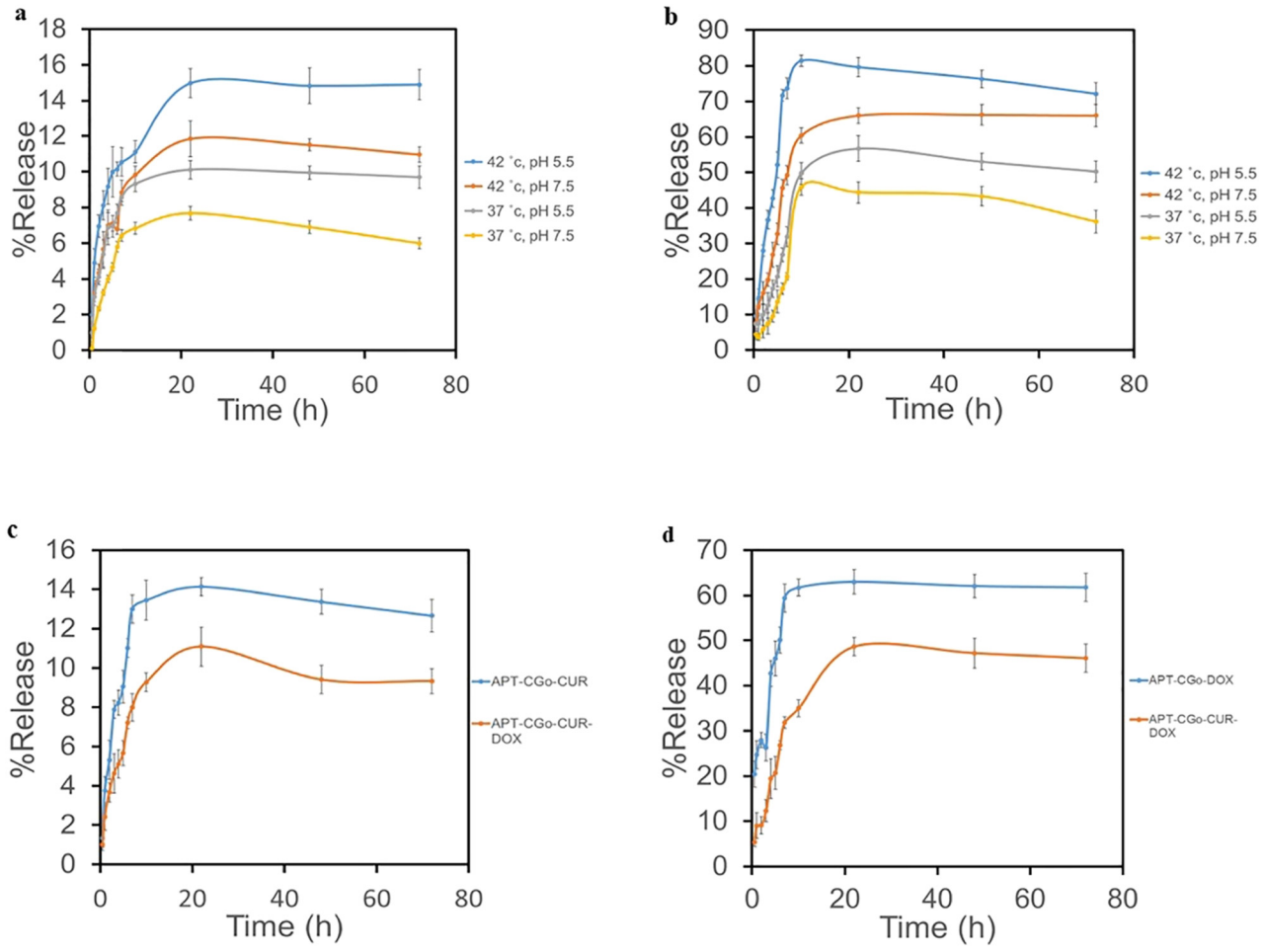

Figure 2: The drug release profile of (a) CUR from APT-CGO-CUR, (b) DOX from APT-CGO-DOX, (c) CUR from APT-CGO-CUR and APT-CGO-CUR-DOX, and (d) DOX from APT-CGO-DOX and APT-CGO-CUR-DOX at pH 7.5, 37°C.

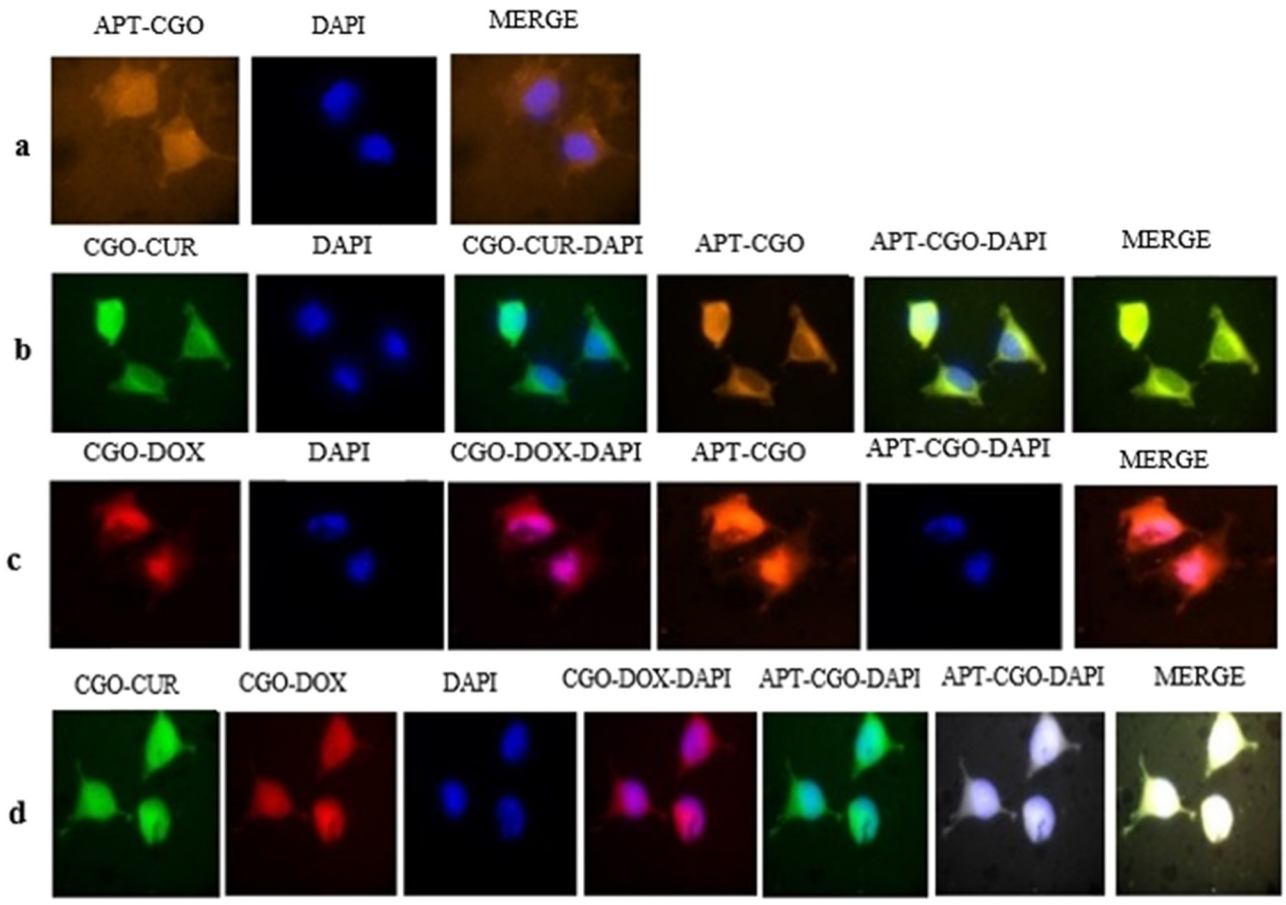

Figure 3: Cellular uptake images of AGS cells, incubated with (a) APT-CGO, (b) APT-CGO-CUR, (c) APT-CGO-DOX, and (d) APT-CGO-CUR-DOX for 180 min. DAPI (blue) was used for nucleus staining.

linked to CGO, weak fluorescence intensity is emitted because of quenching the property of CGO [53]. Although the solubility of CUR as a hydrophobic drug was enhanced through CGO, its release was low leading to weak fluorescence. These results are in good agreement with the results of Zhao *et al.*, which have shown a similar cellular uptake for free CUR and CUR-loaded lipid-polymer hybrid nanoparticles [54].

3.5 Cytotoxicity assay

Although the use of chemotherapeutic agents plays a key role in the treatment of tumor cells, its efficacy has been limited due to broad side effects on noncancerous cells and drug resistance. In fact, cancer cells target multiple pathways to overcome chemotherapy. As a result, combination therapy is a good strategy to overcome drug resistance by targeting several pathways in tumorigenesis [5]. In the current study, CUR and DOX were loaded simultaneously on APT-CGO. The inhibitory effects of free CUR, free DOX, free CGO, APT-CGO, APT-CGO-CUR, APT-CGO-DOX, and APT-CGO-CUR-DOX on the AGS cell line were investigated using MTT assay (Figure 4). Figure 4a shows negligible cytotoxicity of CGOin a dose-dependent manner in the treatment of AGS (all formulations). As shown in Table 3, free CUR and DOX have lower IC_{50} values than that of the loaded form on CGO, while the IC_{50} values of APT-CGO-CUR, APT-CGO-DOX, and APT-CGO-CUR-DOX were very similar to those of free CUR and DOX. When CUR was accompanied with DOX, the cytotoxicity was increased demonstrating an enhancement in cancer treatment efficiency. Interestingly, the current result of the MTT assay was inconsistent with the result of release profiles, that is the cytotoxicity of free CUR and DOX was higher than those of CGO-CUR, CGO-DOX, and CGO-CUR-DOX. In the presence of APT, the toxicity of APT-CGO-CUR, APT-CGO-DOX, and APT-CGO-CUR-DOX was increased due to the targeting property of APT. Although nucleolin is not overexpressed on the surface of all kinds of tumor cells, developing a targeted drug delivery system based on GO, especially for carrying hydrophobic agents, maybe a good option for increasing the

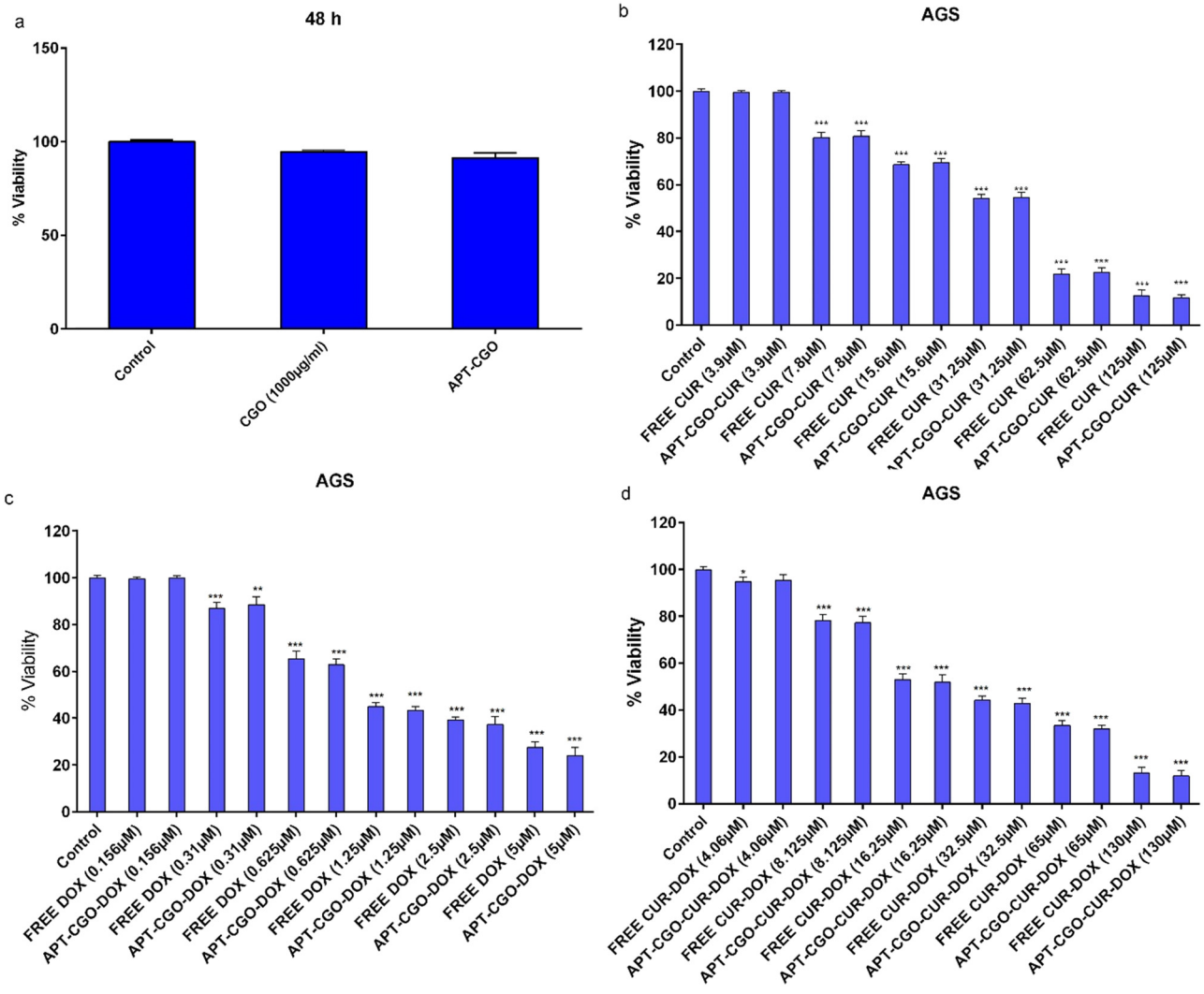

Figure 4: Cytotoxicity analysis of (a) free CGO and APT-CGO in AGS after 48 h. (b) Different concentrations of free CUR and APT-CGO-CUR in AGS after 48 h. (c) Different concentrations of free DOX and APT-CGO-DOX in AGS after 48 h. (d) Different concentrations of free CUR-DOX and APT-CGO-CUR-DOX in AGS after 48 h.

effectiveness of cancer treatment in nucleolin overexpressing cancer cells [55]. Previous studies have improved the efficacy of GO-conjugated PEG used for the delivery of paclitaxel in prostate cancer, nonsmall cell lung cancer (A549), and breast adenocarcinoma (MCF-7) [56,57]. Most anticancer drugs are not able to act on cancer cells specifically, leading to side effects on normal cells; subsequently, targeted drug delivery systems have been designed [58]. AS1411 has reached clinical trials (phases I and II) [59]. After attaching to nucleolin with high affinity, the targeted system can penetrate into some cancer cells such as breast, colorectal, prostate, AGS, and NSCLC [60–62]

3.6 Real-time PCR

The current study evaluated the expression of RB1, CDK2, AKT1, and NF-KB genes, which were involved in different pathways, regulating the survival of cancer cells. As shown in Figure 5, all formulations of free CUR, free

Table 3: IC_{50} values of DOX and CUR on AGS cells after 48 h

IC_{50} (µM)	CUR	DOX	CUR-DOX	APT-CGO-CUR	APT-CGO-DOX	APT-CGO-CUR-DOX
AGS	38.15 ± 3.69	0.88 ± 0.97	17.52 ± 2.80	44.50 ± 4.79	0.64 ± 0.70	14.02 ± 2.86

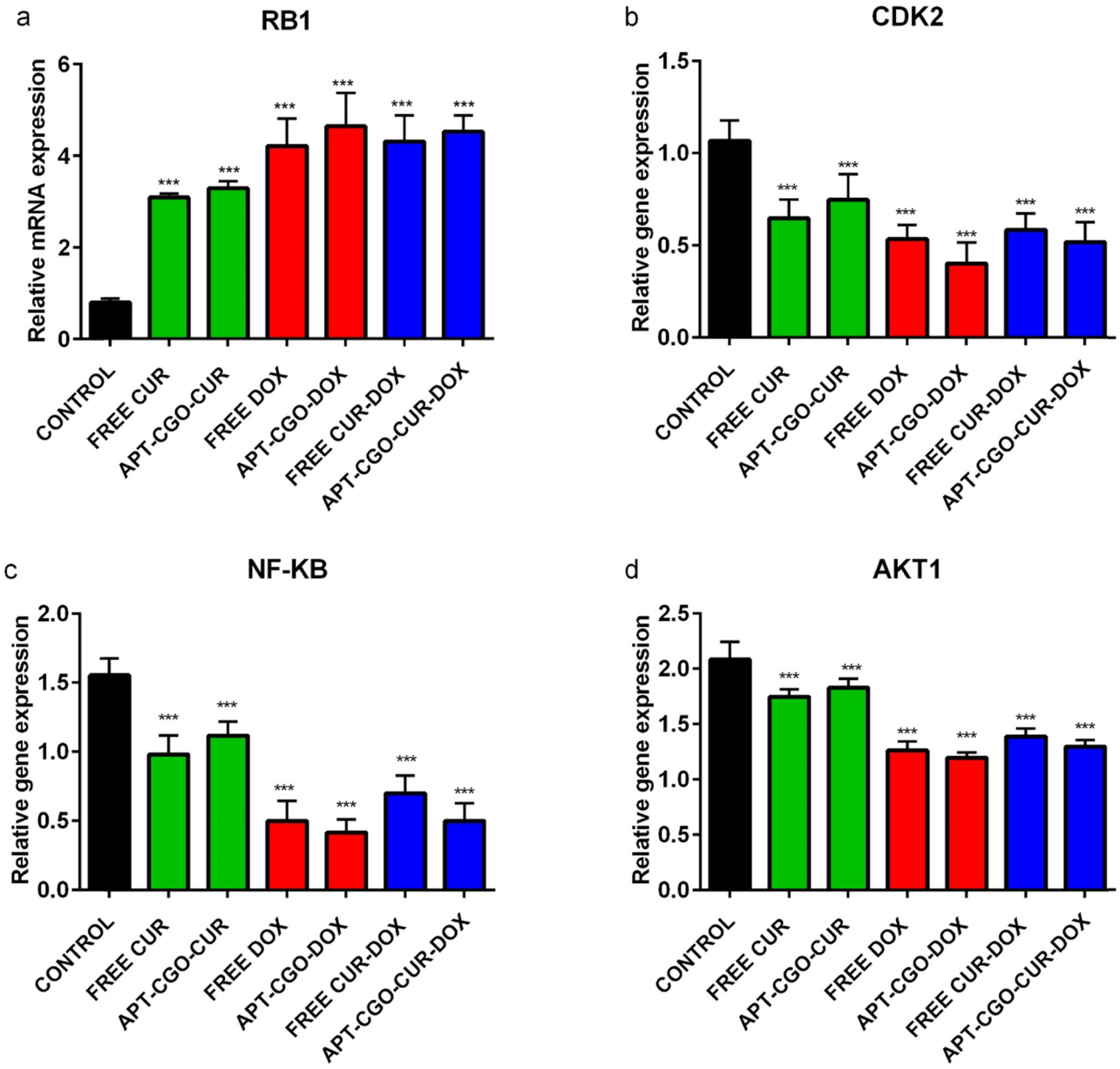

Figure 5: Effect of free CUR, APT-CGO-CUR, free DOX, APT-CGO-DOX, free CUR-DOX, and APT-CGO-CUR-DOX on the expression of (a) RB1 (b) CDK2 (c) NF-KB (d) AKT1 in the AGS cell line after 48 h. Results are expressed as mean ± standard deviation: *$p < 0.05$; **$p < 0.01$; ***$p < 0.001$.

DOX, and APT-CGO-drugs reduced the expression of CDK2, AKT1, and NF-KB genes and increased the expression of RB1 in the treated cells. APT-CGO-CUR, APT-CGO-DOX, and APT-CGO-CUR-DOX have shown similar results to free CUR, free DOX, and free CUR-DOX, respectively. Increased expression of RB1 along with reduced expression of CDK2 monitors the arrest of cells at the G1 phase of the cell cycle. Previous studies displayed that CUR enhanced apoptotic cell death through downregulation of survivin and Bcl2 and upregulation of Bax [63,64]. Also, CUR can induce cell death by induction of ROS [65], suppressing NFKB [66], and activation of death receptors [67]. In another study, CUR decreased the expression of CCNE1, E2F1, and CDK2 while it increased the expression of PTEN inducing cell cycle arrest in the cells treated with CUR. Earlier studies have demonstrated a strong link between the upregulation of CDK inhibitors (p16, p21, and p27) and induction of cell cycle arrest and apoptosis [68,69]. Also, CUR has shown an anti-proliferative effect on Y79 RB cells *via* modulation of miR-26a and upregulation of Rb1 [70]. DOX can motivate two models of cell death by regulating Cdk2 kinase and Cdc2. A low dose of DOX induces cell death by transient activation of Cdk2 kinases, cyclin A, cyclin B, and Cdc2 1-day after the

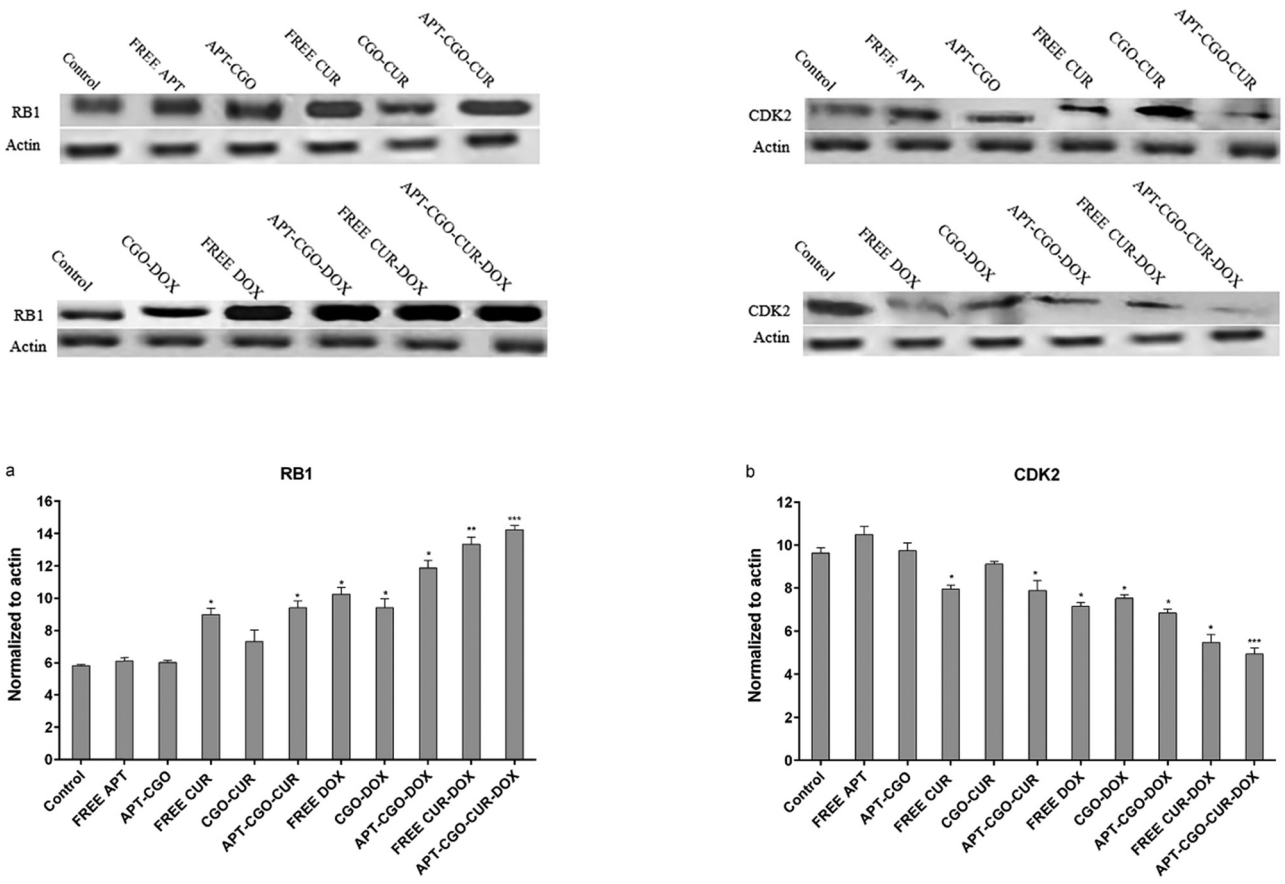

Figure 6: Effect of different formulations on the protein levels of (a) RB1 and (b) CDK2.

treatment. On the other hand, a high dose of DOX causes apoptosis by reducing Cdc2, Cdk2 kinase, cyclin A and cyclin B [71]. The phosphatidylinositol 3-kinase (PI3K)/AKT pathway involved in various cellular processes, including proliferation, survival, metabolism, growth, angiogenesis, and metastasis, was demonstrated in previous research studies [72]. This hyperactivated pathway plays a significant role in the pathogenesis of breast cancer and resistance to chemotherapy [73]. AKT activates NF-κB as its own subset by phosphorylating IκB kinase (IKK), resulting in the release of transcription factor NF-κB from IκB [74]. The hyper-activation of NF-κB has been diagnosed in many types of cancer, such as breast cancer and gastric cancer that suppresses apoptosis [75,76]. In the current study, downregulation of NF-κB in all treated cells may contribute to apoptosis.

3.7 Western blot analysis

Real-time PCR and western blot analyses were conducted to measure the expression of RB1, CDK2, AKT1, NF-KB, RB1, and CDK2 at the levels of gene and protein, respectively. The effect of free APT, APT-CGO, free CUR, free DOX, free CUR-DOX, CGO-CUR, CGO-DOX, APT-CGO-CUR, APT-CGO-DOX, and APT-CGO-CUR-DOX on the expression level of RB1 and CDK2 were evaluated after 48 h (Figure 6). APT-CGO and CGO-CUR did not change the level of RB1 and CDK2 markedly, while free CUR, free DOX, free CUR-DOX, CGO-DOX, APT-CGO-CUR, APT-CGO-DOX, and APT-CGO-CUR-DOX remarkably increased the expression of RB1 compared to untreated controls. Also, the level of RB1 was not changed by free APT compared to APT-containing CGO. Co-delivery of free CUR-DOX by APT-CGO resulted in an enhanced level of RB1 compared to single- and free-form of CUR or APT. Interestingly, the results of western blot analysis were in agreement with the obtained result of RT-PCR (Figure 7).

3.8 Apoptosis analysis

In the current study, the cytotoxicity of the drugs and APT-CGO delivery system was assayed not only by the MTT method but also by an alternative method, Annexin V-FITC/PI double staining. Before probing the cells with

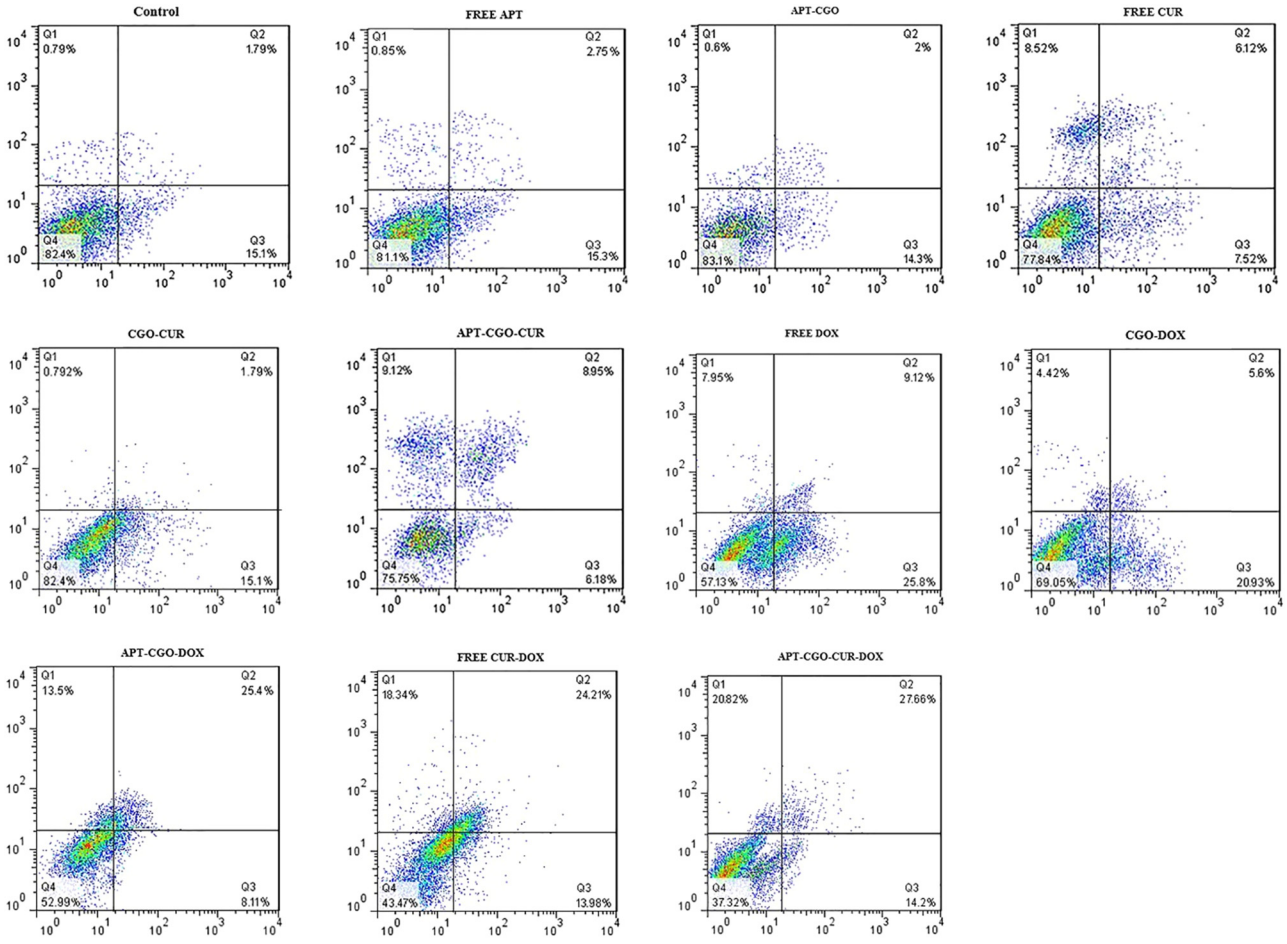

Figure 7: Cell apoptosis evaluated with an Annexin V-FITC kit, after the treatment of cells for 48 h.

flow cytometry analysis, the cells were stained with Annexin VFITC or PI. Figure 7 shows the apoptotic rate of AGS cells. The living cells ($FITC^-/P^-$ or double negative), late apoptotic cells ($FITC^+/PI^+$ or double-positive), early apoptotic cells ($FITC^+/PI^-$) and necrotic cells ($FITC^-/PI^+$) are depicted as Q4, Q3, Q2, and Q1, respectively, in the flow cytometry chart. The apoptosis rates of the cells treated with free APT and APT-CGO were 0.85 and 0.6%, respectively, which were similar to those of the untreated cells (0.79%) because, in this research, a low concentration of biocompatible GO was used. Therefore, the apoptotic effect of this system was negligible. Also, the apoptosis rates of the cells treated with free CUR and free DOX were 8.52 and 7.95% higher than those treated with CGO-CUR (0.89%) and CGO-DOX (4.42%), respectively. However, the apoptosis rate was increased to 9.12 and 13.5%, when the cells were treated with APT-CGO-CUR and APT-CGO-DOX, respectively. When DOX was co-delivered with CUR in free CUR-DOX, the rate of apoptosis was enhanced to 18.34%. Ultimately, the highest cell death rate in all groups was 20.82%, which belonged to APT-CGO-CUR-DOX. These results are consistent with the results of the MTT method. Ramasamy *et al.* co-delivered DOX and quercetin (QC) through pH-sensitive polypeptide-based nanocarriers. The results showed that QC increased the cytotoxic effect of DOX and induced cell apoptosis [77].

4 Conclusion

In this research, CGO as a suitable nanoparticle was selected due to its broad surface and bipolar properties, establishing the co-delivery of CUR and DOX in the AGS cell line. Although the release rate of CUR was less than 15%, the loading efficiency of CUR and DOX was favorable. The release profile was influenced by pH and temperature, which differentiated normal and cancer cells. MTT assay displayed that the IC_{50} values of the drugs loaded on CGO were higher than the free forms, resulting in more capability of drug loading and controlled release, as well as localized delivery, which, in turn, causes fewer

side effects on noncancerous cells. When APT was added to CGO-drugs, the cytotoxicity was increased implying successful targeting of APT to cancer cells. The upregulation of RB1 and downregulation of CDK2, AKT1, and NF-KB genes displayed that cell cycle arrest occurred at the G1 phase. Therefore, the presented results suggested that APT-CGO-CUR-DOX was a promising platform for targeting and combination therapies to enhance the expression of RB1, and to decrease the expression of CDK2, AKT1 and NF-KB genes, and to induce apoptosis. Therefore, this thermosensitive and controlled release of the drug delivery system may be a great option for the treatment of gastric cancer. For enhancing the release rate of CUR and DOX, photodynamic and photothermal therapy can be used in future research work.

Acknowledgements: The authors thank the biochemistry department in Shahid Sadoughi University of Medical Sciences, Iran National Science Foundation, and Herbal Medicine Research Center for financial support.

Funding information: The result of this study was extracted from a PhD thesis that was supported by Shahid Sadoughi University of Medical Sciences (Grant No. 5228) and Iran National Science Foundation (Grant No. 97009563) and Herbal Medicine Research Center (Grant No. 9115).

Author contributions: All authors have accepted responsibility for the entire content of this manuscript and approved its submission.

Conflict of interest: The authors state no conflict of interest.

References

[1] Normanno N, Morabito A, De Luca A, Piccirillo MC, Gallo M, Maiello MR, et al. Target-based therapies in breast cancer: current status and future perspectives. Endocrine-Related Cancer. 2009;16(3):675–702.

[2] Bailar JC, Gornik HL. Cancer undefeated. N Engl J Med. 1997;336(22):1569–74.

[3] Group EBCTC. Effects of chemotherapy and hormonal therapy for early breast cancer on recurrence and 15-year survival: an overview of the randomised trials. Lancet. 2005;365(9472):1687–717.

[4] Dry JR, Yang M, Saez-Rodriguez J. Looking beyond the cancer cell for effective drug combinations. Genome Med. 2016;8(1):125.

[5] Hemati M, Haghiralsadat F, Yazdian F, Jafari F, Moradi A, Malekpour-Dehkordi Z. Development and characterization of a novel cationic PEGylated niosome-encapsulated forms of doxorubicin, quercetin and siRNA for the treatment of cancer by using combination therapy. Artif Cells Nanomed Biotechnol. 2019;47(1):1295–311.

[6] Behzad F, Naghib SM, Tabatabaei SN, Zare Y, Rhee KY. An overview of the plant-mediated green synthesis of noble metal nanoparticles for antibacterial applications. J Ind Eng Chem. 2021;94:92–104.

[7] Askari E, Khoshghadam-Pireyousefan M, Naghib SM, Akbari H, Khosravani B, Zali A, et al. A hybrid approach for in-situ synthesis of bioceramic nanocomposites to adjust the physicochemical and biological characteristics. J Mater Res Technol. 2021;14:464–74.

[8] Kazemi F, Naghib SM, Zare Y, Rhee KY. Biosensing applications of polyaniline (PANI)-based nanocomposites: a review. Polym Rev. 2021;61(3):553–97.

[9] Rahimzadeh Z, Naghib SM, Zare Y, Rhee KY. An overview on the synthesis and recent applications of conducting poly (3, 4-ethylenedioxythiophene) (PEDOT) in industry and biomedicine. J Mater Sci. 2020;55(18):7575–611.

[10] Kalantari E, Naghib SM. A comparative study on biological properties of novel nanostructured monticellite-based composites with hydroxyapatite bioceramic. Mater Sci Eng C. 2019;98:1087–96.

[11] Naghib SM, Behzad F, Rahmanian M, Zare Y, Rhee KY. A highly sensitive biosensor based on methacrylated graphene oxide-grafted polyaniline for ascorbic acid determination. Nanotechnol Rev. 2020;9(1):760–7.

[12] Abtahi NA, Naghib SM, Ghalekohneh SJ, Mohammadpour Z, Nazari H, Mosavi SM, et al. Multifunctional stimuli-responsive niosomal nanoparticles for co-delivery and co-administration of gene and bioactive compound: *in vitro* and *in vivo* studies. Chem Eng J. 2021;429:132090.

[13] Omidinia E, Naghib SM, Boughdachi A, Khoshkenar P, Mills DK. Hybridization of silver nanoparticles and reduced graphene nanosheets into a nanocomposite for highly sensitive L-phenylalanine biosensing. Int J Electrochem Sci. 2015;10(8):6833–43.

[14] Shah N, Chaudhari K, Dantuluri P, Murthy R, Das S. Paclitaxel-loaded PLGA nanoparticles surface modified with transferrin and Pluronic® P85, an *in vitro* cell line and *in vivo* biodistribution studies on rat model. J Drug Target. 2009;17(7):533–42.

[15] Khatibi SA, Misaghi A, Moosavy MH, Basti AA, Koohi MK, Khosravi P, et al. Encapsulation of Zataria multiflora Bioss. essential oil into nanoliposomes and *in vitro* antibacterial activity against Escherichia coli O157: H7. J Food Process Preserv. 2017;41(3):e12955.

[16] Malekimusavi H, Ghaemi A, Masoudi G, Chogan F, Rashedi H, Yazdian F, et al. Graphene oxide-l-arginine nanogel: a pH-sensitive fluorouracil nanocarrier. Biotechnol Appl Biochem. 2019;66(5):772–80.

[17] Mirhosseini M, Shekari-Far A, Hakimian F, Haghiralsadat BF, Fatemi SK, Dashtestani F. Core-shell Au@ Co-Fe hybrid nanoparticles as peroxidase mimetic nanozyme for antibacterial application. Process Biochem. 2020;95:131–8.

[18] Sartipzadeh O, Naghib SM, Shokati F, Rahmanian M, Majidzadeh-A K, Zare Y, et al. Microfluidic-assisted synthesis and modelling of monodispersed magnetic nanocomposites for biomedical applications. Nanotechnol Rev. 2020;9(1):1397–407.

[19] Gooneh-Farahani S, Naghib SM, Naimi-Jamal MR, Seyfoori A. A pH-sensitive nanocarrier based on BSA-stabilized

graphene-chitosan nanocomposite for sustained and prolonged release of anticancer agents. Sci Rep. 2021;11(1):1–14.
[20] Gooneh-Farahani S, Naghib SM, Naimi-Jamal MR. A novel and inexpensive method based on modified ionic gelation for pH-responsive controlled drug release of homogeneously distributed chitosan nanoparticles with a high encapsulation efficiency. Fibers Polym. 2020;21(9):1917–26.
[21] Askari E, Naghib SM, Zahedi A, Seyfoori A, Zare Y, Rhee KY. Local delivery of chemotherapeutic agent in tissue engineering based on gelatin/graphene hydrogel. J Mater Res Technol. 2021;12:412–22.
[22] Foglesong PD, Reckord C, Swink S. Doxorubicin inhibits human DNA topoisomerase I. Cancer Chemother Pharmacol. 1992;30(2):123–5.
[23] Deng G, Chen C, Zhang J, Zhai Y, Zhao J, Ji A, et al. Se@ SiO2 nanocomposites attenuate doxorubicin-induced cardiotoxicity through combatting oxidative damage. Artif Cells Nanomed Biotechnol. 2018;46(sup2):112–21.
[24] Vallianou NG, Evangelopoulos A, Schizas N, Kazazis C. Potential anticancer properties and mechanisms of action of curcumin. Anticancer Res. 2015;35(2):645–51.
[25] Giordano A, Tommonaro G. Curcumin and cancer. Nutrients. 2019;11:10.
[26] Agrawal D, Mishra P. Curcumin and its analogues: potential anticancer agents. Medicinal Res Rev. 2010;30(5):818.
[27] Huun J, Lønning PE, Knappskog S. Effects of concomitant inactivation of p53 and pRb on response to doxorubicin treatment in breast cancer cell lines. Cell Death Discovery. 2017;3(1):1–6.
[28] Pourjavadi A, Asgari S, Hosseini SH, Akhlaghi M. Codelivery of hydrophobic and hydrophilic drugs by graphene-decorated magnetic dendrimers. Langmuir. 2018;34(50):15304–18.
[29] Mohanty C, Das M, Sahoo SK. Emerging role of nanocarriers to increase the solubility and bioavailability of curcumin. Expert Opin Drug Delivery. 2012;9(11):1347–64.
[30] Tiwari H, Karki N, Pal M, Basak S, Verma RK, Bal R, et al. Functionalized graphene oxide as a nanocarrier for dual drug delivery applications: the synergistic effect of quercetin and gefitinib against ovarian cancer cells. Colloids Surf B, Biointerfaces. 2019;178:452–9.
[31] Huang X, Yin Z, Wu S, Qi X, He Q, Zhang Q, et al. Graphene-based materials: synthesis, characterization, properties, and applications. Small. 2011;7(14):1876–902.
[32] Karki N, Tiwari H, Pal M, Chaurasia A, Bal R, Joshi P, et al. Functionalized graphene oxides for drug loading, release and delivery of poorly water soluble anticancer drug: a comparative study. Colloids Surfaces B Biointerfaces. 2018;169:265–72.
[33] Gholami A, Emadi F, Nazem M, Aghayi R, Khalvati B, Amini A, et al. Expression of key apoptotic genes in hepatocellular carcinoma cell line treated with etoposide-loaded graphene oxide. J Drug Delivery Sci Technol. 2020;57:101725.
[34] Wu S, Zhao X, Cui Z, Zhao C, Wang Y, Du L, et al. Cytotoxicity of graphene oxide and graphene oxide loaded with doxorubicin on human multiple myeloma cells. Int J Nanomed. 2014;9:1413.
[35] Charmi J, Nosrati H, Amjad JM, Mohammadkhani R, Danafar H. Polyethylene glycol (PEG) decorated graphene oxide nanosheets for controlled release curcumin delivery. Heliyon. 2019;5(4):e01466.
[36] Muthoosamy K, Abubakar IB, Bai RG, Loh H-S, Manickam S. Exceedingly higher co-loading of curcumin and paclitaxel onto polymer-functionalized reduced graphene oxide for highly potent synergistic anticancer treatment. Sci Rep. 2016;6:32808.
[37] Motlagh NSH, Parvin P, Mirzaie ZH, Karimi R, Sanderson JH, Atyabi F. Synergistic performance of triggered drug release and photothermal therapy of MCF7 cells based on laser activated PEGylated GO + DOX. Biomed Opt Express. 2020;11(7):3783–94.
[38] Lu Y, Wu P, Yin Y, Zhang H, Cai C. Aptamer-functionalized graphene oxide for highly efficient loading and cancer cell-specific delivery of antitumor drug. J Mater Chem B. 2014;2(24):3849–59.
[39] Alibolandi M, Mohammadi M, Taghdisi SM, Ramezani M, Abnous K. Fabrication of aptamer decorated dextran coated nano-graphene oxide for targeted drug delivery. Carbohydr Polym. 2017;155:218–29.
[40] Taghavi S, Nia AH, Abnous K, Ramezani M. Polyethylenimine-functionalized carbon nanotubes tagged with AS1411 aptamer for combination gene and drug delivery into human gastric cancer cells. Int J Pharmaceutic. 2017;516(1–2):301–12.
[41] Honary S, Zahir F. Effect of zeta potential on the properties of nano-drug delivery systems-a review (Part 2). Tropical J Pharm Res. 2013;12(2):265–273.
[42] Mishra B, Patel BB, Tiwari S. Colloidal nanocarriers: a review on formulation technology, types and applications toward targeted drug delivery. Nanomed Nanotechnol Biol Med. 2010;6(1):9–24.
[43] Pourjavadi A, Asgari S, Hosseini SH. Graphene oxide functionalized with oxygen-rich polymers as a pH-sensitive carrier for co-delivery of hydrophobic and hydrophilic drugs. J Drug Delivery Sci Technol. 2020;56:101542.
[44] Motlagh NH, Parvin P, Mirzaie Z, Karimi R, Sanderson J, Atyabi F. Synergistic performance of triggered drug release and photothermal therapy of MCF7 cells based on laser activated PEGylated GO + DOX. Biomed Opt Express. 2020;11(7):3783–94.
[45] Yang X, Zhang X, Liu Z, Ma Y, Huang Y, Chen Y. High-efficiency loading and controlled release of doxorubicin hydrochloride on graphene oxide. J Phys Chem C. 2008;112(45):17554–58.
[46] Wang K, Zhang C, Bao J, Jia X, Liang Y, Wang X, et al. Synergistic chemopreventive effects of curcumin and berberine on human breast cancer cells through induction of apoptosis and autophagic cell death. Sci Rep. 2016;6(1):1–14.
[47] Li H, Zhang N, Hao Y, Wang Y, Jia S, Zhang H, et al. Formulation of curcumin delivery with functionalized single-walled carbon nanotubes: characteristics and anticancer effects *in vitro*. Drug Delivery. 2014;21(5):379–87.
[48] Swietach P, Vaughan-Jones RD, Harris AL, Hulikova A. The chemistry, physiology and pathology of pH in cancer. Philos Trans R Soc B Biol Sci. 2014;369(1638):20130099.
[49] Dinarvand R, Sepehri N, Manoochehri S, Rouhani H, Atyabi F. Polylactide-co-glycolide nanoparticles for controlled delivery of anticancer agents. Int J Nanomed. 2011;6:877.
[50] Malekmohammadi S, Hadadzadeh H, Farrokhpour H, Amirghofran Z. Immobilization of gold nanoparticles on folate-conjugated dendritic mesoporous silica-coated reduced graphene oxide nanosheets: a new nanoplatform for curcumin

pH-controlled and targeted delivery. Soft Matter. 2018;14(12):2400–10.
[51] Omidi S, Pirhayati M, Kakanejadifard A. Co-delivery of doxorubicin and curcumin by a pH-sensitive, injectable, and *in situ* hydrogel composed of chitosan, graphene, and cellulose nanowhisker. Carbohydr Polym. 2020;231:115745.
[52] Lee RJ, Wang S, Turk MJ, Low PS. The effects of pH and intraliposomal buffer strength on the rate of liposome content release and intracellular drug delivery. Biosci Rep. 1998;18(2):69–78.
[53] Motlagh NSH, Parvin P, Refahizadeh M, Bavali A. Fluorescence properties of doxorubicin coupled carbon nanocarriers. Appl Opt. 2017;56(26):7498–503.
[54] Zhao Y, Lin D, Wu F, Guo L, He G, Ouyang L, et al. Discovery and *in vivo* evaluation of novel RGD-modified lipid-polymer hybrid nanoparticles for targeted drug delivery. Int J Mol Sci. 2014;15(10):17565–76.
[55] Liu J, Wei T, Zhao J, Huang Y, Deng H, Kumar A, et al. Multifunctional aptamer-based nanoparticles for targeted drug delivery to circumvent cancer resistance. Biomaterials. 2016;91:44–56.
[56] Thapa RK, Youn YS, Jeong J-H, Choi H-G, Yong CS, Kim JO. Graphene oxide-wrapped PEGylated liquid crystalline nanoparticles for effective chemo-photothermal therapy of metastatic prostate cancer cells. Colloids Surf B Biointerfaces. 2016;143:271–7.
[57] Xu Z, Wang S, Li Y, Wang M, Shi P, Huang X. Covalent functionalization of graphene oxide with biocompatible poly (ethylene glycol) for delivery of paclitaxel. ACS Appl Mater Interfaces. 2014;6(19):17268–76.
[58] Iversen T-G, Skotland T, Sandvig K. Endocytosis and intracellular transport of nanoparticles: present knowledge and need for future studies. Nano Today. 2011;6(2):176–85.
[59] Mongelard F, Bouvet P. AS-1411, a guanosine-rich oligonucleotide aptamer targeting nucleolin for the potential treatment of cancer, including acute myeloid leukemia. Curr Op Mol Therapeutics. 2010;12(1):107–14.
[60] Liao Z-X, Chuang E-Y, Lin C-C, Ho Y-C, Lin K-J, Cheng P-Y, et al. An AS1411 aptamer-conjugated liposomal system containing a bubble-generating agent for tumor-specific chemotherapy that overcomes multidrug resistance. J Controlled Rel. 2015;208:42–51.
[61] Tang Y, Hu H, Zhang MG, Song J, Nie L, Wang S, et al. An aptamer-targeting photoresponsive drug delivery system using "off–on" graphene oxide wrapped mesoporous silica nanoparticles. Nanoscale. 2015;7(14):6304–10.
[62] Zhong Y, Meng F, Deng C, Zhong Z. Ligand-directed active tumor-targeting polymeric nanoparticles for cancer chemotherapy. Biomacromolecules. 2014;15(6):1955–69.
[63] Subramaniam D, Ponnurangam S, Ramamoorthy P, Standing D, Battafarano RJ, Anant S, et al. Curcumin induces cell death in esophageal cancer cells through modulating Notch signaling. PLoS One. 2012;7(2):e30590.
[64] Yang J, Cao Y, Sun J, Zhang Y. Curcumin reduces the expression of Bcl-2 by upregulating miR-15a and miR-16 in MCF-7 cells. Med Oncol. 2010;27(4):1114–8.
[65] Ismail NI, Othman I, Abas F, Lajis H, Naidu N, R. Mechanism of apoptosis induced by curcumin in colorectal cancer. Int J Mol Sci. 2019;20(10):2454.
[66] Zheng M, Ekmekcioglu S, Walch ET, Tang C-H, Grimm EA. Inhibition of nuclear factor-κB and nitric oxide by curcumin induces G2/M cell cycle arrest and apoptosis in human melanoma cells. Melanoma Res. 2004;14(3):165–71.
[67] Bush JA, Cheung Jr K-JJ, Li G. Curcumin induces apoptosis in human melanoma cells through a Fas receptor/caspase-8 pathway independent of p53. Exp Cell Res. 2001;271(2):305–14.
[68] Park M-J, Kim E-H, Park I-C, Lee H-C, Woo S-H, Lee J-Y, et al. Curcumin inhibits cell cycle progression of immortalized human umbilical vein endothelial (ECV304) cells by up-regulating cyclin-dependent kinase inhibitor, p21WAF1/CIP1, p27KIP1 and p53. Int J Oncol. 2002;21(2):379–83.
[69] Srivastava RK, Chen Q, Siddiqui I, Sarva K, Shankar S. Linkage of curcumin-induced cell cycle arrest and apoptosis by cyclin-dependent kinase inhibitor p21/WAF1/CIP1. Cell Cycle. 2007;6(23):2953–61.
[70] Bai J, Guo D, Liu X. Curcumin inhibits retinoblastoma cell proliferation by miR-26a targeting the tumor suppressor gene Rb1 in Y79 cells. J Anal Oncol. 2020;9(1):63–71.
[71] Park SS, Eom Y-W, Choi KS. Cdc2 and Cdk2 play critical roles in low dose doxorubicin-induced cell death through mitotic catastrophe but not in high dose doxorubicin-induced apoptosis. Biochem Biophys Res Commun. 2005;334(4):1014–21.
[72] Ooms LM, Binge LC, Davies EM, Rahman P, Conway JR, Gurung R, et al. The inositol polyphosphate 5-phosphatase PIPP regulates AKT1-dependent breast cancer growth and metastasis. Cancer Cell. 2015;28(2):155–69.
[73] Clark AR, Toker A. Signalling specificity in the Akt pathway in breast cancer. Biochem Soc Trans. 2014;42(5):1349–55.
[74] Vandermoere F, El Yazidi-Belkoura I, Adriaenssens E, Lemoine JM, Hondermarck H. The antiapoptotic effect of fibroblast growth factor-2 is mediated through nuclear factor-κ B activation induced *via* interaction between Akt and I κ B kinase-β in breast cancer cells. Oncogene. 2005;24(35):5482–91.
[75] DeGraffenried L, Chandrasekar B, Friedrichs W, Donzis E, Silva J, Hidalgo M, et al. NF-κB inhibition markedly enhances sensitivity of resistant breast cancer tumor cells to tamoxifen. Ann Oncol. 2004;15(6):885–90.
[76] Lin K, Rong Y, Chen D, Zhao Z, Bo H, Qiao A, et al. Combination of ruthenium complex and doxorubicin synergistically inhibits cancer cell growth by down-regulating PI3K/AKT signaling pathway. Front Oncol. 2020;10:141.
[77] Ramasamy T, Ruttala HB, Chitrapriya N, Poudal BK, Choi JY, Kim ST, et al. Engineering of cell microenvironment-responsive polypeptide nanovehicle co-encapsulating a synergistic combination of small molecules for effective chemotherapy in solid tumors. Acta Biomaterialia. 2017;48:131–43.